PAPER

Electronic and surface properties of PbS nanoparticles exhibiting efficient multiple exciton generation

Samantha J. O. Hardman,*[a] **Darren M. Graham,**[a] **Stuart K. Stubbs,**[a] **Ben F. Spencer,**[a,b] **Elaine A. Seddon,**[a] **Ho-Ting Fung,**[a] **Sandra Gardonio,**[c‡] **Fausto Sirotti,**[d] **Mathieu G. Silly,**[d] **Javeed Akhtar,**[e§] **Paul O'Brien,**[e] **David J. Binks**[a] **and Wendy R. Flavell.**[a]

Ultrafast transient absorption measurements have been used to study multiple exciton generation in solutions of PbS nanoparticles vigorously stirred to avoid the effects of photocharging. The threshold and slope efficiency of multiple exciton generation are found to be $2.5\pm0.2\times E_g$ and 0.34 ± 0.08, respectively. Photoemission measurements as a function of nanoparticle size and ageing show that the position of the valence band maximum is pinned by surface effects, and that a thick layer of surface oxide is rapidly formed at the nanoparticle surfaces on exposure to air.

1. Introduction

The theoretical maximum efficiency of single junction solar cells under unconcentrated sunlight is currently limited to ca. 30% by the rapid cooling of the hot carriers produced by the absorption of photons with energy in excess of the band gap.[1] However, photovoltaic (PV) devices based on nanoparticles (NPs) may be able to exceed this limit by making use of multiple exciton generation (MEG), also known as carrier multiplication (CM), where the excess energy of an absorbed photon is used to generate extra electron-hole pairs rather than being wasted as heat. MEG has been observed spectroscopically in a number of different NPs including CdSe,[2] CdTe,[3] CdSe/CdTe,[4] InP,[5] InAs,[6] PbSe,[7] PbS,[7] PbTe,[8] and Si.[9] Moreover, photoconductive[10] and photovoltaic[11] devices incorporating PbS NPs which exhibit MEG have also been reported recently, and PbS NPs are the subject of the study presented here. Previous investigations of MEG in PbS NPs[7, 12-14] have reported quantum yield (QY) values which differed significantly, varying from ~110% to ~280% for approximately the same ratio of photon energy (hv) to band gap (E_g). Most of these studies were conducted before it became apparent that photocharging of samples can lead to erroneous QY values because the spectroscopic signature of a single exciton in a charged NP is similar to that of biexciton in a neutral NP.[15-17] However, it has recently been shown that rapidly stirring[15, 16] or flowing[17] a solution of NPs can prevent this effect, leading to reliable QY values. A very recent study[14] was largely performed on static samples of PbS NPs but did present a typical transient obtained when the sample was static and compared it to one obtained when the sample was flowing. From this comparison, the authors estimated that photocharging could account for ~10% of the apparent QY in their samples.

The advantages of generating more than one electron-hole pair per incident photon through MEG are lost if those carriers cannot be extracted from the NP to contribute to a photocurrent. It is therefore important to determine the electronic structure and chemistry of the interface between the NP and its surroundings. In use in a device, the NPs are typically sandwiched between suitable photoanode and photocathode materials in a solid state device. As the size of a NP decreases its band gap increases, due to the quantum confinement effect, and the surface:volume ratio increases. Because small nanoparticles have such a high surface:volume ratio the properties of this interface and of the NP surface may dominate the characteristics of the NP. X-ray photoelectron spectroscopy (XPS) is therefore a very suitable technique for the study of NPs, as it is sensitive to only the first few layers of a surface. There has been some investigation of the effects of surface chemistry on the properties of nanoparticle samples.[18] It is now clear that the choice of capping ligand may affect not only the stability and solubility of the nanoparticles, but also the local vacuum level,[19] and the optical properties of the sample,[18] while the substrate upon which the nanoparticles are deposited may pin the energy of the highest occupied molecular orbital (HOMO).[20] It is therefore clear that issues of surface chemistry and preparation have an important effect on the energy level line-up of the nanoparticle/substrate interface, a crucial parameter in PV design as it affects the efficiency of charge extraction.[21] Previous XPS studies of PbS nanoparticles have shown that the species present at the surface depends on the choice of ligand,[22] and that oxidation products may be found at the surface.[23] Indeed, in the case of PbSe nanoparticles this oxidation is found to transform 50% of the nanoparticle volume within 24 hours.[24] Surface states are predicted to have a strong effect on the rate of relaxation of hot carriers by impact ionisation, thus affecting MEG,[25] although recent experiments on PbSe suggest that the effect on MEG efficiency is not marked.[24] It seems clear, therefore, that it is important to probe not only whether or not MEG can be observed, but also whether or not the

surface and interface properties of the NPs allow MEG to be used. In this study we use ultrafast transient absorption spectroscopy to determine the threshold and slope efficiency of MEG in stirred solutions of PbS NPs. We then use photoemission to investigate the electronic structure and surface composition of a range of PbS NPs that show efficient MEG, deposited on photoanode substrates. We investigate how the surface composition changes with exposure to air, and consider the implications for carrier dynamics.

2. Experimental

PbS NP samples were prepared by a novel environmentally-benign method, using olive oil as both solvent and capping agent, as described in detail elsewhere.[23] Briefly, PbO and TMS (bistrimethylsilyl sulfide) were dissolved separately in olive oil. Rapid injection of the TMS solution into the PbO solution resulted in development of the NPs. By varying growth time and concentration of TMS NPs of a specific size could be produced. The PbS NPs were precipitated by the addition of anhydrous acetone and subsequent centrifugation. The material obtained was then re-dissolved in dry toluene and re-precipitated as before. It was found that the long-chain olive oil capping groups of the as-prepared samples were highly insulating and so unsuitable for a device requiring charge injection into or extraction from the NP. Exchanging these ligands for butylamine or 3-mercaptopropionic acid resulted in samples free from charging effects during the photoemission experiments indicating that charge transport to and from the NP was possible.

For the transient absorption experiments the dynamics of the lowest energy (1S) absorption peak were measured using a home-built transient absorption spectrometer described previously.[5] In short, a white light continuum probe beam was a generated in a 2 mm-thick sapphire window by 0.8 – 2 µJ of the output of a Ti:Sapphire ultrafast regenerative amplifier operating at a centre wavelength of 800 nm with ~100 fs pulses and a repetition rate of 1 kHz. The NP samples, in hexane or chloroform, were contained in 10 mm path length quartz cuvettes, and were stirred using a magnetic stirrer (Thermo Scientific Variomag Mini) at 1000 rpm unless otherwise stated. For probe wavelengths less than 1.2 eV the probe beam was split into reference and sample beams which were balanced, in the absence of any sample photo-excitation, using a variable neutral density filter wheel before being passed through a monochromator and detected with a pair of silicon photodiodes. For probe wavelengths over 1.2 eV, beyond the spectral range of the silicon photodiodes, the entire probe beam passed through the sample and the monochromator and was detected by an InGaAs photodiode (FGA21, Thorlabs Inc.). The majority of the output from the regenerative amplifier was used to pump an optical parametric amplifier, and associated non-linear frequency conversion stages were used to generate a pump beam. The pump beam was modulated with a mechanical chopper synchronized to the 2nd sub-harmonic of the laser repetition rate before exciting the sample. The photodiode signals were sampled using a digital lock-in amplifier and the time delay between pump and probe beams was controlled by a motorized optical delay line. Four olive-oil-capped PbS NP samples with 1S absorption peaks at 1.4, 1.3, 1.1 and 1.0 eV and estimated diameters ranging

from 3.4 to 4.7 nm[26] were investigated. The NP samples had absorbances at the 1S peak (A, calculated using the natural logarithm) of 0.48, 0.57, 0.49, and 0.35 respectively.

The XPS experiments were carried out both on the SuperESCA beamline at the ELETTRA synchrotron, Italy, and on the TEMPO beamline at the SOLEIL synchrotron, France. The electron energy analysers used were a hemispherical electron energy analyzer with 150 mm mean radius and a Scienta SES2002 respectively, both equipped with delay-line detectors. Photoemission spectra were recorded at room temperature and a typical total resolution of 180 meV was estimated from a Fermi edge spectrum recorded from a clean metal surface. Four butylamine-capped PbS nanoparticle samples with 1S absorption features (effective band gaps) of 1.7, 1.4, 1.2, and 1.0 eV and estimated diameters of 2.7, 3.3, 3.8, and 4.6 nm respectively[26] were deposited on tin-doped indium oxide (ITO) coated glass. A 3-mercaptopropionic-acid-capped PbS nanoparticle sample, with a 1S absorption features at 1.0 eV and an estimated diameter of 4.6 nm[26] was deposited onto an m-plane ZnO single crystal. The spectra were referenced to a metallic Fermi edge and normalised to the incident photon energy (I_0) where appropriate. A Shirley-type background was subtracted from the photoemission spectra and a sum of Gaussian and Lorentzian functions with 50% Lorentzian character was used to fit the line shapes, as recommended in the literature.[27] The spin-orbit splitting of the doublets was set as 4.9 eV for the Pb 4f peaks and 1.2 eV for the S 2p peaks.

3. Results and Discussion

3.1. Multiple Exciton Generation

Figure 1 compares the fractional change in transmission, $\Delta T/T$, transients induced in the 1.3 eV band gap sample by pump photons of 2.5 and 5.2 eV, i.e. 1.9 and $4.0 \times E_g$ respectively. It can be seen that when pumping with $1.9 \times E_g$ photons, when there is insufficient photon energy for MEG to occur, there are no features other than a long-lived decay. The single-exciton lifetime of olive-oil-capped PbS NPs is approximately 1 µs,[23] much longer than the 500 ps time window monitored in this work, and thus the signal associated with a single-exciton decay appears as a
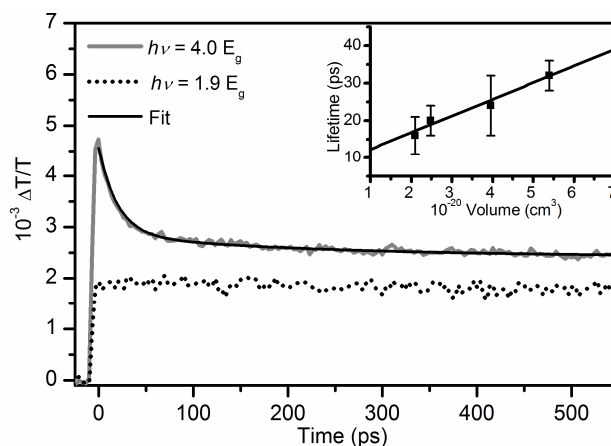
Fig. 1 Main panel: Transmittance transients induced in the Eg=1.3 eV NP sample by pumping at a photon energies corresponding to 1.9 and $4.0 \times E_g$. Inset: Biexciton lifetime as a function of NP volume.

flat plateau. In contrast, when a NP absorbs more than one photon, a biexciton decay transient in addition to the single-exciton plateau is observed[7] due to the fast Auger recombination process.[28, 29] The absence of such a feature when using pump energies of $1.9 \times E_g$ shows that for the fluences used the probability of a NP absorbing more than one photon per pulse is small. This is consistent with a calculated estimate of the average number of photons absorbed by a NP per pump pulse, <N>, for this transient. <N> can be estimated from the experimentally obtained values of $\Delta T(0)/T$, which are approximately equal to the changes in absorbance, ΔA, for small values. The fractional change in absorbance, $\Delta A/A$, corresponds to the occupation number of the conduction band minimum (CBM) i.e. the ratio of <N> and the degeneracy of the conduction band minimum[28] (8 for PbS[13]). Hence, for PbS <N> is approximately $(8A^{-1}) \Delta T(0)/T$, and thus equals 0.03 for the data shown. In contrast, the transient induced by $4.0 \times E_g$ energy photons includes, in addition to the plateau associated with the single exciton, a short-lived decay feature which is characteristic of a biexciton in such strongly confined NPs. We attribute this feature to MEG for the following two reasons. Firstly <N> for this transient is less than 0.06 so this decay feature cannot be due to multiple absorptions per pulse. Secondly, vigorous stirring has previously been shown to effectively suppress photocharging[15, 16] which can otherwise produce a similar decay feature. To confirm that the stirring rate used here is sufficient to suppress photocharging additional transients were obtained at a range of stirring rates (see ESI†). Photocharging is not significant for all NP types, for example little difference is observed between stirred and unstirred samples of InP NPs,[5] but it is evident that, as with PbSe NPs,[15-17] photocharging has a significant effect on the exciton dynamics of PbS NPs in unstirred solutions.

The large difference between single and biexciton lifetimes affords a means by which MEG QYs can be readily determined. The method of analysis used in this work, derived from earlier methods[9, 30] has been explained in detail by Stubbs et al.[5] but is briefly described here. Small values of $\Delta T/T$ measured at the 1S absorption peak are proportional to the exciton number density in the sample.[31] The initial value of $\Delta T/T$ thus represents the exciton number density created by the pump pulse, while its value at a time much longer than the biexciton lifetime, τ_{BX}, but much shorter than the single-exciton lifetime corresponds to the number of initially photoexcited NPs. The ratio of these two values, R, thus represents the average number of excitons created per initially photoexcited NP, and can be found by fitting an exponential decay with a time constant of τ_{BX} to the recorded transient. Most transients were well described by a single exponential but a few, particularly those obtained at high fluence and high photon energy, showed evidence of an additional slow decay on a timescale of approximately $10\tau_{BX}$. In these cases, the effect of this additional decay could be accounted for either by fitting a single exponential just to the first 100 ps of the transient or by fitting a biexponential decay to the whole transient and using only the component associated with τ_{BX} in the calculation of R. The value of τ_{BX} found for each NP is plotted against NP volume (assuming a spherical shape) in the inset of Figure 1. The biexciton lifetime is seen to increase linearly with volume, in agreement with results reported previously and is attributed to the enhancement of Auger recombination by quantum confinement. In the limit of vanishing fluence, the probability of a NP absorbing more than one photon is negligible and thus at this limit, R equals the average number of excitons created per absorbed photon i.e. the MEG QY. Figure 2 shows R as a function of initial $\Delta T/T$ for the four samples studied and includes
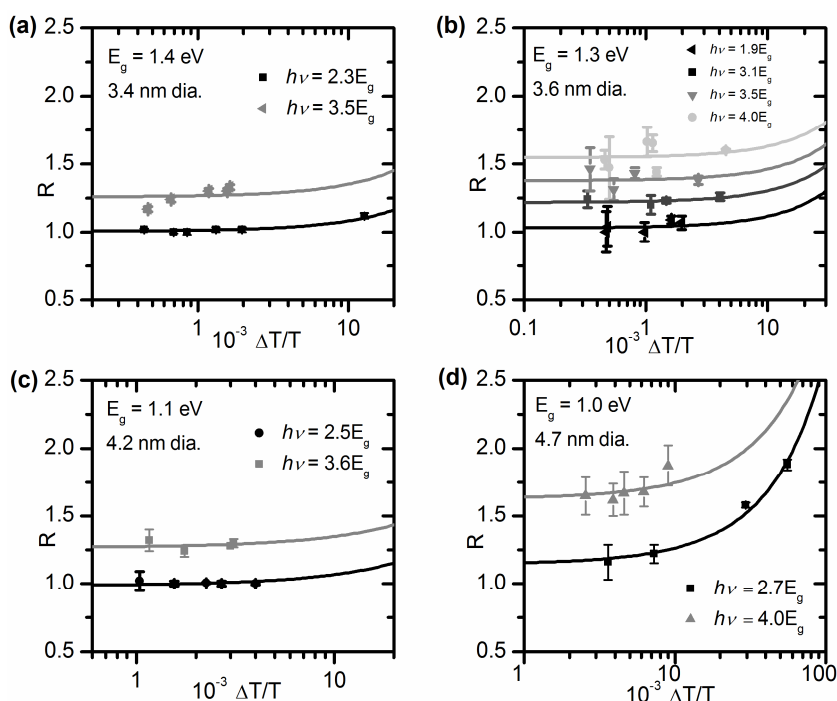
Fig.2. Average number of excitons generated per photoexcited NP, R, as function of initial fractional change in transmission, $\Delta T/T$, for samples with band gaps, Eg, of: (a) 1.4 eV excited with pump photon energies 2.3 (black) and 3.5 (grey) times Eg , (b) 1.3 eV excited with pump photon energies 1.9 (black), 3.1 (dark grey), 3.5 (grey) and 4.0 (light grey) times Eg , (c) 1.1 eV excited with pump photon energies 2.5 (black) and 3.6 (grey) times Eg , (d) 1.0 eV excited with pump photon energies 2.7 (black) and 4.0 (grey) times Eg. The lines shown are fitted to equation (1) with free parameter QY.

PAPER

fits to the following expression:[5]

$$R = k\frac{\Delta T(0)}{T}\left[1 - \exp\left(-\frac{k}{QY}\frac{\Delta T(0)}{T}\right)\right]^{-1} \quad (1)$$

where $k=8A^{-1}$ and is a constant. In all cases where the photon energy is less than ~2.5×E_g, R tends to unity as $\Delta T/T$ decreases. However, when the photon energy is more than ~2.5×E_g, R is greater than unity at levels of fluence where the probability of biexciton production by multiple photon absorption is insignificant, indicating that MEG occurs at these pump energies.

Figure 3 shows the number of additional excitons created by MEG, i.e. QY-1, against pump photon energy normalised to the band gap. Assuming the excess photon energy, $h\upsilon$-E_g, is partitioned between the electron and hole according to their relative effective masses, the threshold photon energy required for MEG to occur, $h\upsilon_{th}$, is given by:[32]

$$h\nu_{th} = E_g\left(2 + \frac{m_e^*}{m_h^*}\right) \quad (2)$$

for $m_h^* > m_e^*$, where m_e^* and m_h^* are the electron and hole effective masses respectively. For bulk PbS the ratio of m_h^*/m_e^* has been reported to be approximately 0.6,[33] using this value the threshold photon energy for PbS NPs is expected to be ~2.6×E_g.
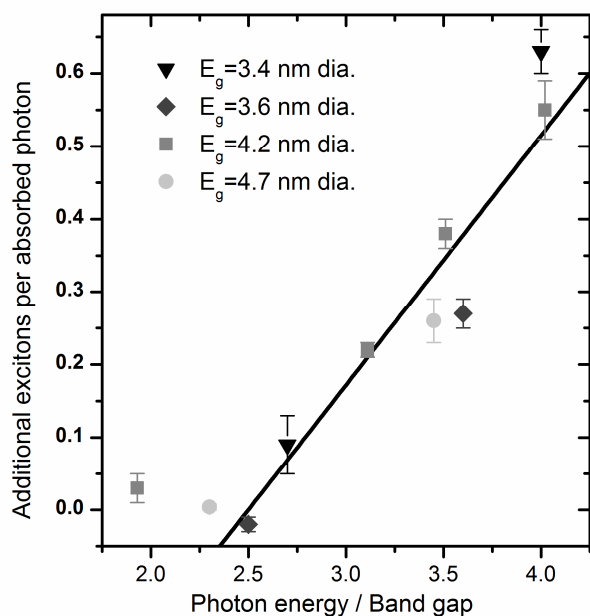
Fig.3. The additional number of excitons produced per absorbed photon by MEG as a function of $h\upsilon/E_g$ for samples with band gaps of 1.0, 1.1, 1.3, and 1.4 eV.

A linear fit to those points above 2.6×E_g yielded a threshold of 2.5±0.2×E_g, which is consistent with the energy partition model,

and a slope efficiency of η=0.34±0.08. The observation of a threshold in agreement with equation (2) strongly supports the attribution of these results to MEG rather than photocharging; only the MEG mechanism would have a threshold that is dependent on E_g and not just hv. Schaller et al.[12] and Ellingson et al.[7] have reported results for PbS NPs consistent with a threshold of ~2.6×E_g but with much greater slope efficiencies (of η~1.0). However, both of these studies were conducted before the importance of sample stirring to avoid photocharging results was known. The values of hv$_{th}$ and η for stirred or flowed PbSe NP solutions reported recently[15-17] are very similar to those found here for PbS NPs. The enhancement of photocurrent by MEG in PbS NPs reported by Sambur et al.[11] was also found to have a threshold of 2.5±0.25×E_g, although η was measured to be somewhat higher at about 0.7. The most recently reported assessment of MEG in PbS NP[14] found similar values of hv$_{th}$ and η for NPs of approximately the same size as those studied here. Interestingly, they also reported that the value of hv$_{th}$/E_g reduced with decreasing NP size. However, as Fig. 3 shows, we observe no indication of similar size dependence in this work, or of a significantly different QY for NPs of different diameters but excited at the same value of $h\nu/E_g$.

Beard et al.[34] have recently presented an analysis of MEG in which the following relationship between threshold and slope efficiency was derived under the assumption that MEG is the dominant relaxation mechanism for hot electrons:
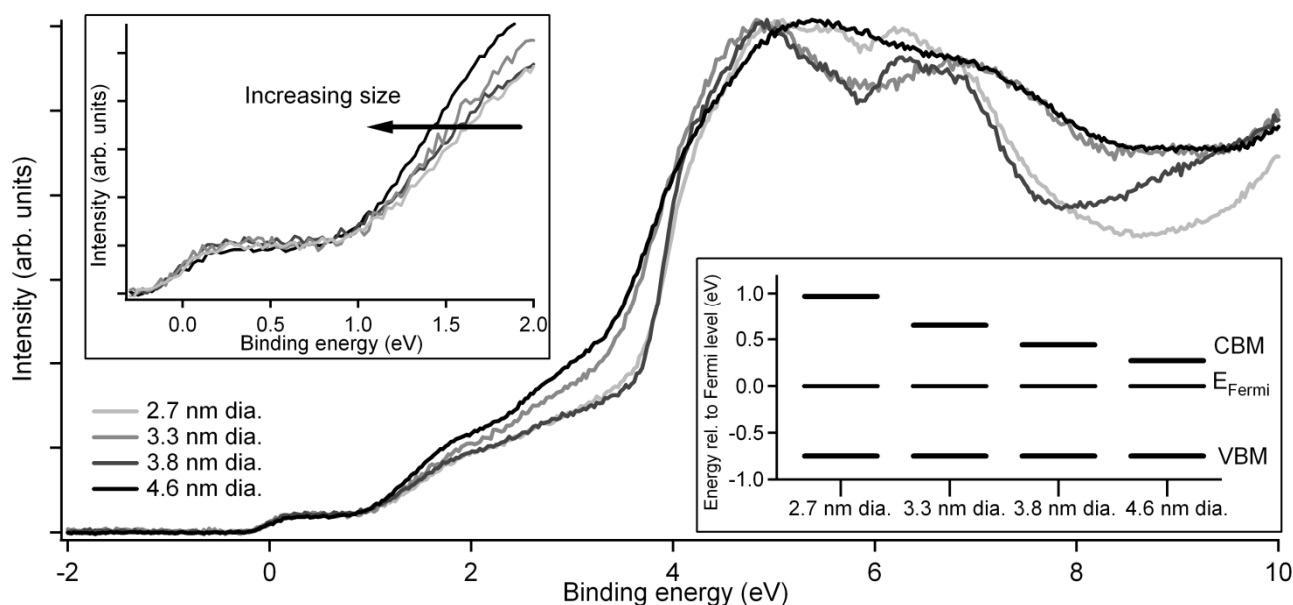
$$h\nu_{th} = E_g\left(1 + \eta^{-1}\right) \quad (3).$$

However, they also found that when other relaxation processes became competitive with MEG then η is determined instead by the relative rates of MEG and these competing processes. The values for $h\nu_{th}$ and η found in this study do not satisfy Eqn. 3 indicating that in this case the rate of MEG is similar to that of other relaxation processes. In contrast, the results reported by Sambur et al.[11] do satisfy Eqn. 3 and thus suggest MEG is dominant. One possible explanation for this difference in behaviour, as noted by Sambur et al.,[11] is that the dielectric environment of the PbS NPs in the photocurrent measurements was significantly different from that typically used in spectroscopic measurements and that this reduced the rate of relaxation by processes other than MEG. In particular, whilst, as is the case in this study, spectroscopic measurements are usually performed on isolated NPs in an organic solvent and passivated by long-chain hydrocarbons, the NPs used in the photocurrent measurements were passivated by a short-chain ligand and adsorbed onto a TiO$_2$ crystal in an aqueous environment.

3.2. Electronic Structure

As noted above, the MEG yield may be influenced by the environment of the NPs, and the observation of MEG in solution does not guarantee that the additional carriers can be extracted

from the NP. Of key importance to extraction are the positions of the valence band maximum (VBM) and the conduction band minimum (CBM) of the NP, relative to the surrounding photoanode and photocathode materials. The optical measurements may be usefully combined with photoemission spectra to determine these frontier orbital energies as a function of nanoparticle size. Valence band spectra for 4 sizes of NP deposited on ITO substrates are shown in Fig 4. The main part of the valence band, lying between ca. 4 and 8 eV binding energy (BE) contains mainly contributions from the ligands. The features that may be ascribed to the PbS valence band lie at lower energies, in the range 1 – 5 eV BE,[23] and it is here that we may expect to see the effects of quantum confinement, as the band gap, and hence the position of the valence band maximum (VBM) changes with nanoparticle size. The feature at a binding energy of zero is attributed to metallic lead, arising from decomposition of PbS (discussed further in section 3.3) and provides a convenient reference point.

Fig.4. Photoemission spectra of the valence band of 4 sizes of butylamine-capped PbS nanoparticles deposited on ITO-coated glass. Insets show an enlargement of the valence band edge region and a diagram of the positions of the conduction band minimum (CBM) and valence band maximum (VBM) relative to the Fermi energy (E_{Fermi}). The CBM position is inferred from optical absorption data. The X-ray photon energy is 250 eV.

As can be seen from the figure, there is a slight shift of the valence band edge (at around 1 - 1.5 eV BE) towards the Fermi energy with increase in nanoparticle size (inset, Fig. 4, top). However, the change in the VBM position is within experimental error; the extrapolated VBM position is 0.75±0.1 eV for all samples. Any shift in VBM position is at most 0.1 eV. This is very similar in magnitude to that observed by Carlson et al.[20] for CdSe nanoparticles adsorbed on ZnO, and much smaller (by a factor of at least 10) than that expected on the basis of the simplest model of quantum confinement. This model predicts that the shifts of the VBM and the conduction band minimum (CBM) are inversely proportional to m_h^* and m_e^* respectively, and are given by

$$\Delta E_{VBM} = \frac{-h^2}{8m_h^* r^2}, \quad \Delta E_{CBM} = \frac{h^2}{8m_e^* r^2} \quad (4)$$

where h is Planck's constant and r is the radius of the quantum dot. As the ratio of the hole and electron effective masses in PbS is around 0.6.[33] Eqn. 4 predicts the downward shift of the CBM with increasing nanoparticle size to be smaller than the upward shift of the VBM. The bottom inset to Fig. 4 shows the energy level diagrams arrived at by using the VBM measured from photoemission, together with the 1S exciton energy from optical absorption measurements (taking this to give an approximate measure of the position of the CBM). It is clear that the system deviates strongly from Eqn. 4, with a significant movement of the CBM, while the VBM appears to be almost pinned, analogous to the effect measured by Carlson *et al.*[20] in CdSe. Such pinning to the VBM or Fermi level of an adjacent material requires direct electronic interaction, which in the case of CdSe, is suggested to be with the ZnO substrate, assuming the NPs are incompletely encapsulated by the ligands.[20] In our case we find that this effect is independent of the substrate used (we have repeated the experiment using a gold substrate, see ESI†), and thus we believe that the pinning may be due to electronic interaction with the ligand (or surface degradation products – see section 3.3) rather than the substrate. One consequence is that as the diameter of the nanoparticles increases the Fermi level moves relatively closer to the conduction band than the valence band, and thus the nanoparticles become effectively more n-type as the diameter increases, tending towards behaviour of bulk PbS.[35] The VBM pinning has no influence on the MEG threshold (which is dependent on the band gap), or its measurement in solution for isolated NPs here. However, it may effect the overall yield and hence η if the interface interaction leads to the creation of new surface states that affect the hot carrier relaxation rate,[25] as discussed in section 3.1. The surface properties of the nanoparticles are therefore examined below in section 3.3. More

importantly, the position of the CBM is crucial to the subsequent electron extraction from the nanoparticle, as the photoexcited carriers must be injected from this level into (typically) the conduction band of an n-type oxide such as ZnO or TiO$_2$. Thus optimisation of the CBM position is just as important as optimisation of the QY for MEG. The VBM pinning observed in this work (Fig. 4) suggests carrier injection will be significantly less efficient than expected on the basis of an effective mass model for nanoparticles with diameters larger than around 3 nm.[36]

3.3. Surface chemistry

A further effect that may impair the efficiency of carrier extraction (and also the MEG yield) is the surface chemistry of the nanoparticles. Here we examine the surface chemistry of the nanoparticles described in section 3.2, and how this evolves with time. Four sizes of butylamine-capped nanoparticle were deposited onto ITO-coated glass, and transferred to a UHV environment within a few hours. Using an X-ray photon energy of 250 eV, corresponding to a photoelectron inelastic mean free path of 0.55 nm[37] and a corresponding sampling depth of 1.65 nm, the Pb 4f and S 2p core level spectra shown in Fig. 5 (a) – (h) were recorded. It can be seen that all the spectra are complex, arising in each case from several sets of doublets associated with different chemical species. The S 2p core level shows particularly large chemical shifts, such that any structure observed between ca. 165 eV BE and 171 eV BE may be attributed to oxidised species (such as sulfate and sulfite). It is immediately clear, therefore, that oxidised species are found in all the samples. The species present are assigned as neutral lead, neutral sulfur, lead and sulfur as found in PbS, and lead and sulfur as found in oxidised species PbSO$_x$. The peak positions and assignments are shown in table 1 and are in agreement with previous values reported for PbS nanoparticles.[22, 38] The sampling depth used in this experiment is fairly small compared with the diameter of the nanoparticles, so this experiment probes the surface layers of the nanoparticles in the main. It is clear that a significant proportion of oxidised species is found for every particle size. As the size of the nanoparticle increases, the proportion of oxide present appears to decrease somewhat (most clearly seen in the S 2p spectra of Fig. 5). By normalising the spectra using the photoionisation cross sections[39] it is possible to calculate the relative amount of species present in the samples. Using the S 2p peaks we find ratios of PbSO$_x$:PbS of 1.0±0.1:1, 1.0±0.1:1, 0.5±0.1:1 and 0.5±0.1:1 for the four samples with estimated diameters of 2.7, 3.3, 3.8 and 4.6 nm respectively. The proportion of oxides present appears largest for the smaller nanoparticles.

This is consistent with the larger surface-to-volume ratio of these nanoparticles, assuming that we probe mainly the surface layers in this experiment. We investigate this further below by varying the sampling depth in the experiment. We believe that the neutral Pb and S could arise from rapid initial photodegradation under the intense X-ray beam at SuperESCA (as we have not observed these species in experiments at lower photon density SR sources, discussed further below); however, these signals did not increase further in intensity during our experiments. The presence of metallic lead provides a useful internal Fermi level reference, as seen in section 3.2. In all cases we find a Pb:S ratio of around 3:1, much larger than the expected 1:1. This is consistent with
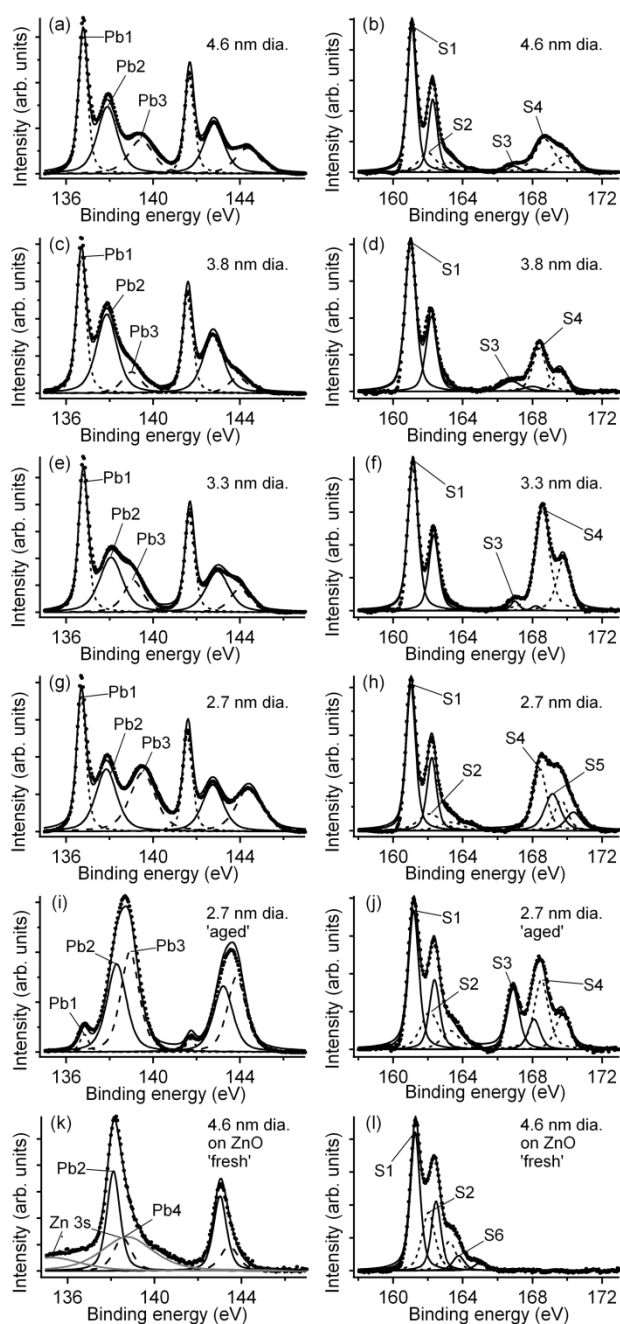
Fig. 5. X-ray photoemission spectra Pb 4f (left) and S 2p (right) core levels for: (a) and (b) 4.6 nm, (c) and (d) 3.8 nm, (e) and (f) 3.3 nm, and (g) and (h) 2.7 nm diameter butylamine-capped nanoparticle samples deposited on ITO-coated glass, sampled with photoelectron kinetic energy of approximately 100 eV (photon energy 250 eV); (i) and (j) a 2.7 nm diameter butylamine-capped nanoparticle sample deposited on ITO coated glass which was exposed to air for ca. 1 week between deposition and study, sampled with photoelectron kinetic energy of approximately 100 eV (photon energy 250 eV); (k) and (l) a 4.6 nm diameter 3-mercaptopropionic-acid-capped nanoparticle sample deposited on ZnO, sampled with kinetic energy of approximately 80 eV (photon energy 230 eV). Species present are neutral lead (Pb1, long dashes), lead as found in PbS (Pb2, line), lead as found in PbSOx (Pb3, dots), lead attached to the capping ligand (Pb4, dots), sulfur as found in PbS (S1, line), neutral sulfur (S2, dots), sulfur as found in oxidised PbSOx (S3, line, S4, dots, and S5, line), and sulfur as found in the capping ligand (S6, dashes).[22, 38, 40, 41]

photodegradation of PbS to Pb, with the more volatile S being lost to the vacuum.

**Table 1.** Components of Pb 4f and S 2p core level peak fitting with assignment and binding energy. [22, 38, 40, 41]

Component	Assigment	Binding Energy (eV) ±0.1 eV
Pb1	neutral Pb	136.8 & 141.7
Pb2	lead in PbS	138.0 & 142.9
Pb3	lead in PbSOx	139.1 & 144.0
Pb4	lead in PbS linked to capping ligand	138.5 & 143.4
S1	sulfur in PbS	161.1 & 162.3
S2	neutral sulfur	162.0 & 163.2
S3	sulfur in PbSOx(sulfite)	166.9 & 168.1
S4	sulfur in PbSOx (sulfate)	168.6 & 169.8
S5	sulfur in PbSOx	169.2 & 170.4
S6	capping ligand	163.8 & 165.0

The reaction of nanoparticle surfaces with the atmosphere is an effect which has been previously observed in PbS.[22] To investigate this, we deposited a sample of the 2.7 nm butylamine-capped nanoparticles onto a substrate approximately one week before the experiments took place, and then stored the sample in air. The Pb 4f and S 2p core level spectra for this sample are shown in Fig. 5(i) – (j). In comparison to the spectra of the same sample without a long exposure to air, shown in Fig. 5(g) – (h), it is clear that significant surface oxidation has occurred (an increase in components Pb3, S3,4, Table 1). Using the S 2p peaks we find the ratio of PbSOx:PbS of 1.2±0.1:1 after ageing (Fig. 5(j)), compared to 1.0±0.1:1 for the sample transferred to UHV in a few hours (Fig. 5(h)). The proportion of neutral lead is also significantly lower after ageing, perhaps suggesting that the presence of surface PbSO$_4$ passivates the PbS against photodegradation. Overall the results suggest that the nanoparticles become oxidised in a relatively short period on exposure to air.

In our work, we have also investigated routes to preparing PbS nanoparticles that are chemically bound to a suitable n-type oxide, such as ZnO, into which photoexcited electrons may be injected. Here, after synthesis in olive oil, ligand exchange was carried out with 3-mercaptopropionic acid in order to chemically link the nanoparticles to a ZnO single crystal substrate, using the approach of Carlson *et al.*[20] The Pb 4f and S 2p core level spectra are shown in Fig. 5(k) – (l). A Zn 3s peak from the substrate is also visible in the Pb 4f region. In marked contrast to the butylamine-capped samples there are no signals due to any oxidised species (particularly clear in the S 2p spectrum, Fig. 5(l)). The speed of deposition is thought to be the main contributing factor to this, as the deposited sample was exposed to air for less than a minute before insertion into UHV. By comparing with data for the butylamine-capped samples (Fig. 5), it appears that significant oxidation occurs after aerial exposures of less than an hour. In addition to the lead and sulfur species attributed to the PbS, there are also species present attributed to S in the capping group,[42] Pb on the surface of the nanoparticle linked to the capping group,[22] and also some neutral S (Table 1). However, there is a striking absence of neutral Pb. These data were acquired at the TEMPO beamline at SOLEIL, using lower photon density than at SuperESCA, so less photodegradation may

have occurred. However, we cannot rule out the possibility that neutral Pb is a product of surface ageing, along with oxidised species.
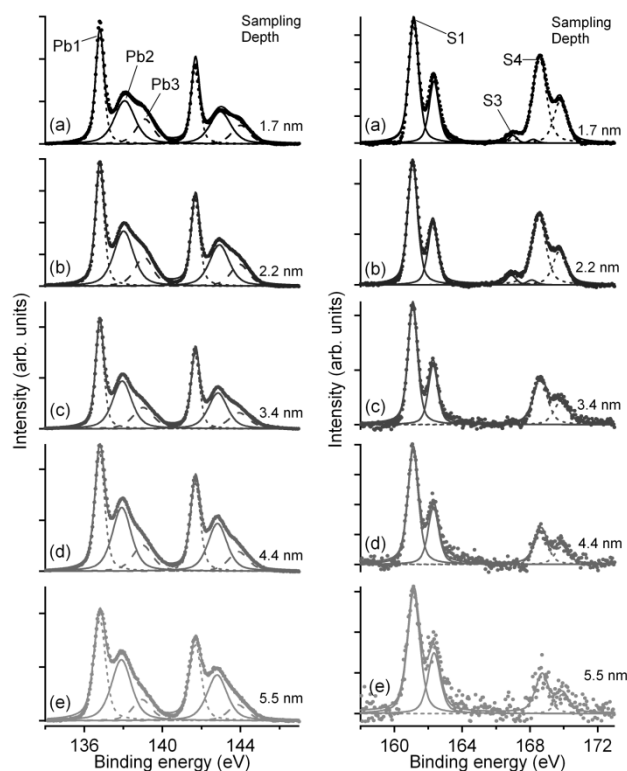
Fig. 6. X-ray photoemission spectra of Pb 4f (left) and S 2p (right) core levels for the 3.3 nm diameter nanoparticle sample deposited on ITO-coated glass at kinetic energies of approximately 100 (a), 200 (b), 400 (c), 600 (d) and 800 (e) eV (photon energies 250, 350, 550, 750 and 950 eV respectively). Species present are neutral lead (Pb1, long dashes), lead as found in PbS (Pb2, line), lead as found in PbSOx (Pb3, dots), sulfur as found in PbS (S1, line), and sulfur as found in PbSOx (S3, line and S4, dots).

We may probe the distribution of the products of nanoparticle ageing within the nanoparticle by varying the incident photon energy in photoemission experiments, and hence the photoelectron kinetic energy, which determines the photoelectron inelastic mean free path. The sampling depth from which 95% of the detected electrons originate is approximately 3 times the inelastic mean free path.[43] Photoemission spectra of the Pb 4f and S 2p core levels at varying incident photon energies for the 3.3 nm diameter nanoparticle sample (used to generate Fig. 5(e) and (f)) are shown in Fig. 6. The kinetic energy of the detected electrons ranged from 100 to 800 eV, which gives inelastic mean free path values from 0.55 to 1.82 nm,[37] and corresponding sampling depths between 1.65 and 5.46 nm. The species present are lead and sulfur as found in PbS, lead and sulfur as found in PbSOx, and also a large proportion of neutral lead (Table 1). On increasing the sampling depth the Pb:PbS ratio remains approximately constant at around 1:1, but the percentage of sulfur and lead present as oxidised components reduces by around 50% over the full range of depths probed, suggesting that these oxidised components are present at the nanoparticle surfaces (Figure 6 and Table 2[44]). The ratio of Pb:S, using only the signals originating from PbS, varied from 2.4±0.1:1 at the smallest

sampling depth to 1.2±0.1:1 at the largest. As the flux of photoelectrons is attenuated according to the Beer-Lambert law as it emerges from the sample, it is possible to obtain an estimate of the thickness of the oxidised layer by a simple model[45] using the integrated peak intensities and inelastic mean free paths.[37] A simple 'two-layer' model, where the oxidised species (assumed to be sulfate) are assumed to form a uniform layer only at the surface gives a value of 0.5 ± 0.2 nm for the depth of the oxide layer. This is significant compared with the diameter of the core of the nanoparticle (3.3 nm).

Table 2. Ratio of the concentrations of oxidised to non-oxidised species, [PbSOx]/[PbS], obtained from S 2p and Pb 4f core levels at a range of sampling depths for the 3.3 nm diameter nanoparticle sample deposited on ITO-coated glass.

Photon energy (Sampling depth)	[PbSOx]/[PbS]	
	S 2p	Pb 4f
250 eV (1.7 nm)	1.0±0.1	0.5±0.1
350 eV (2.2 nm)	0.8±0.1	0.5±0.1
550 eV (3.4 nm)	0.6±0.1	0.5±0.1
750 eV (4.4 nm)	0.4±0.1	0.4±0.1
950 eV (5.5 nm)	0.3±0.2	0.3±0.1

In summary, the PbS nanoparticles undergo rapid degradation on exposure to air, forming a surface layer of PbSOx (typically sulfate with some sulfite) that is thick compared with typical nanoparticle diameters. In the case of the 3.3 nm nanoparticle shown in Figure 6, approximately two-thirds of the volume of the nanoparticle has been converted to oxidised species after a few hours' exposure to air. The degradation happens rapidly, on timescales of minutes, but continues on timescales of weeks. This rapid and very significant oxidative degradation is strikingly similar to that observed recently in PbSe,[24] where a 50% conversion to oxide was observed after exposure to air for 24 hours. The formation of a substantial insulating layer at the surface of the nanoparticles might be expected to be undesirable for efficient charge extraction, but in fact has been recently observed to suppress charge carrier recombination, reducing charge loss through this route.[21] However, it may undesirable for the long-term stability of devices based on PbS, unless the oxide layer is conformal around the core, passivating the surface. It also means that as a function of time, the central PbS core of the nanoparticle will contract in diameter as its surfaces oxidise. If this happens, its band gap will increase (as has been observed in PbSe[24]), and the efficiency of MEG (for a fixed input photon energy) will decrease, as the threshold for MEG is determined by the band gap. We have observed a shift of the VBM to higher binding energy, consistent with an increase in band gap, for the 2.7 nm 'aged' NP discussed earlier (see ESI†). Following ligand-exchange for photoemission, the NPs are unfortunately highly insoluble and therefore not amenable to further absorption measurements. However, we have consistently observed a blue-shift in the 1S absorption threshold for the initially-synthesised olive-oil-capped NPs, when stored in solution for extended periods (see ESI†). At the very least, the rapid surface degradation of the nanoparticles adds some ambiguity to the determination of nanoparticle size and the correlation of this with optical properties including the threshold for MEG. We suggest

that this factor (in addition to experimental issues such as stirring speed) may contribute to the spread of exciton multiplicity values previously observed.

4. Conclusions

We have presented a study of the MEG efficiency of PbS NPs in which the samples have been stirred to avoid photocharging. The values of MEG quantum yield and slope efficiency thus found are smaller than those reported by several previous spectroscopic studies undertaken before the importance of photocharging was understood, and are similar to those found recently for PbSe NP samples that have also been stirred or flowed.[15-17] The slope efficiency was also less than both that reported in a recent study using photocurrent measurements[11] and that predicted by an analysis[34] under the assumption that MEG is the dominant cooling process for hot electrons. We attribute the reduced efficiency in our case to the chemical and electronic environment experienced by the NPs introducing alternate electron cooling pathways which are competitive with MEG. We have investigated the electronic structure and chemistry of the interface between the PbS NPs and their surroundings when adsorbed onto suitable photoanode materials (ITO and ZnO), in order to investigate whether or not the additional carriers generated by MEG may be extracted efficiently. The position of the valence band maximum of the PbS NPs does not change significantly with NP size, and appears to be pinned relative to the Fermi energy (we suggest, by interaction with the ligand or surface degradation products). This effect will produce carrier injection that is significantly less efficient than expected on the basis of an effective mass model for NPs with diameters larger than around 3 nm. The NPs undergo rapid degradation on exposure to air, forming a surface layer of PbSOx that is thick compared with typical NP diameters (typically of the order of 0.5 nm). This may lead to an apparent rise in MEG threshold (and drop in quantum yield) as a function of time, as the core of the PbS nanoparticle contracts. Thus we conclude that while PbS NPs show efficient MEG, work is necessary to control their surface chemistry before its benefits are fully realised.

Notes and references

[a] School of Physics and Astronomy and the Photon Science Institute, University of Manchester, Oxford Road, Manchester M13 9PL, UK. E-mail:samantha.hardman@manchester.ac.uk

b Cockcroft Institute, Daresbury Science and Innovation Campus, Warrington, Cheshire WA4 4AD, UK.

c SuperESCA beamline, Sincrotrone Trieste S.C.p.A., S.S. 14 Km 163.5, 34012 Basovizza, Trieste, Italy.

5 *d TEMPO beamline, Société civile Synchrotron SOLEIL, L'Orme des Merisiers, Saint-Aubin - BP 48, 91192 Gif-sur-Yvette, France.*

e School of Chemistry, University of Manchester, Oxford Road, Manchester M13 9PL, UK

1. W. Shockley and H. J. Queisser, *Journal of Applied Physics*, 1961, 20 **32**, 510-519.

2. R. D. Schaller, M. A. Petruska and V. I. Klimov, *Applied Physics Letters*, 2005, **87**, 253102.

3. Y. Kobayashi, T. Udagawa and N. Tamai, *Chemistry Letters*, 2009, **38**, 830-831.

25 4. D. Gachet, A. Avidan, I. Pinkas and D. Oron, *Nano Letters*, 2010, **10**, 164-170.

5. S. K. Stubbs, S. J. O. Hardman, D. M. Graham, B. F. Spencer, W. R. Flavell, P. Glarvey, O. Masala, N. L. Pickett and D. J. Binks, *Physical Review B*, 2010, **81**, 081303(R).

30 6. R. D. Schaller, J. M. Pietryga and V. I. Klimov, *Nano Letters*, 2007, **7**, 3469-3476.

7. R. J. Ellingson, M. C. Beard, J. C. Johnson, P. R. Yu, O. I. Micic, A. J. Nozik, A. Shabaev and A. L. Efros, *Nano Letters*, 2005, **5**, 865-871.

35 8. J. E. Murphy, M. C. Beard, A. G. Norman, S. P. Ahrenkiel, J. C. Johnson, P. R. Yu, O. I. Micic, R. J. Ellingson and A. J. Nozik, *Journal of the American Chemical Society*, 2006, **128**, 3241-3247.

9. M. C. Beard, K. P. Knutsen, P. R. Yu, J. M. Luther, Q. Song, W. K. Metzger, R. J. Ellingson and A. J. Nozik, *Nano Letters*, 2007, **7**, 40 2506-2512.

10. V. Sukhovatkin, S. Hinds, L. Brzozowski and E. H. Sargent, *Science*, 2009, **324**, 1542-1544.

11. J. B. Sambur, T. Novet and B. A. Parkinson, *Science*, 2010, **330**, 63-66.

45 12. R. D. Schaller, M. Sykora, J. M. Pietryga and V. I. Klimov, *Nano Letters*, 2006, **6**, 424-429.

13. G. Nair, S. M. Geyer, L. Y. Chang and M. G. Bawendi, *Physical Review B*, 2008, **78**, 125325.

14. G. Nootz, L. A. Padilha, L. Levina, V. Sukhovatkin, S. Webster, L. 50 Brzozowski, E. H. Sargent, D. J. Hagan and E. W. Van Stryland, *Physical Review B*, 2011, **83**, 7.

15. J. A. McGuire, J. Joo, J. M. Pietryga, R. D. Schaller and V. I. Klimov, *Accounts of Chemical Research*, 2008, **41**, 1810-1819.

16. J. A. McGuire, M. Sykora, J. Joo, J. M. Pietryga and V. I. Klimov, 55 *Nano Letters*, 2010, **10**, 2049-2057.

17. A. G. Midgett, H. W. Hillhouse, B. K. Hughes, A. J. Nozik and M. C. Beard, *Journal of Physical Chemistry C*, 2010, **114**, 17486-17500.

18. D. J. Asunskis, I. L. Bolotin, J. E. Haley, A. Urbas and L. Hanley, *Journal of Physical Chemistry C*, 2009, **113**, 19824-19829.

60 19. A. M. Munro, B. Zacher, A. Graham and N. R. Armstrong, *ACS Applied Materials & Interfaces*, 2010, **2**, 863-869.

20. B. Carlson, K. Leschkies, E. S. Aydil and X. Y. Zhu, *Journal of Physical Chemistry C*, 2008, **112**, 8419-8423.

21. N. Zhao, T. P. Osedach, L.-Y. Chang, S. M. Geyer, D. Wanger, M. T. 65 Binda, A. C. Arango, M. G. Bawendi and V. Bulovic, *ACS Nano*, 2010, **4**, 3743-3752.

22. A. Lobo, T. Moller, M. Nagel, H. Borchert, S. G. Hickey and H. Weller, *Journal of Physical Chemistry B*, 2005, **109**, 17422-17428.

23. J. Akhtar, M. A. Malik, P. O'Brien, K. G. U. Wijayantha, R. 70 Dharmadasa, S. J. O. Hardman, D. M. Graham, B. F. Spencer, S. K. Stubbs, W. R. Flavell, D. J. Binks, F. Sirotti, M. El Kazzi and M. Silly, *Journal of Materials Chemistry*, 2010, **20**, 2336-2344.

24. M. Sykora, A. Y. Koposov, J. A. McGuire, R. K. Schulze, O. Tretiak, J. M. Pietryga and V. I. Klimov, *ACS Nano*, 2010, **4**, 2021-2034.

75 25. G. Allan and C. Delerue, *Physical Review B*, 2009, **79**, 5.

26. L. Cademartiri, E. Montanari, G. Calestani, A. Migliori, A. Guagliardi and G. A. Ozin, *Journal of the American Chemical Society*, 2006, **128**, 10337-10346.

27. R. Hesse, P. Streubel and R. Szargan, *Surface and Interface Analysis*, 80 2007, **39**, 381-391.

28. V. I. Klimov, *Journal of Physical Chemistry B*, 2000, **104**, 6112-6123.

29. V. I. Klimov, A. A. Mikhailovsky, D. W. McBranch, C. A. Leatherdale and M. G. Bawendi, *Science*, 2000, **287**, 1011-1013.

85 30. R. D. Schaller and V. I. Klimov, *Physical Review Letters*, 2004, **92**.

31. V. I. Klimov, *Semiconductor and Metal Nanocrystals*, Marcel Dekker, New York, 2004.

32. M. C. Beard and R. J. Ellingson, *Laser & Photonics Reviews*, 2008, **2**, 377-399.

90 33. D. R. Lide, ed., *Handbook of Physics and Chemistry*, CRC Press, Boca Raton, FL, 2009.

34. M. C. Beard, A. G. Midgett, M. C. Hanna, J. M. Luther, B. K. Hughes and A. J. Nozik, *Nano Letters*, 2010, **10**, 3019-3027.

35. W. W. Scanlon, *Journal of Physics and Chemistry of Solids*, 1959, **8**, 95 423-428.

36. B. R. Hyun, Y. W. Zhong, A. C. Bartnik, L. F. Sun, H. D. Abruna, F. W. Wise, J. D. Goodreau, J. R. Matthews, T. M. Leslie and N. F. Borrelli, *ACS Nano*, 2008, **2**, 2206-2212.

37. S. Tanuma, C. J. Powell and D. R. Penn, *Surface and Interface* 100 *Analysis*, 1991, **17**, 927-939.

38. D. J. Asunskis and L. Hanley, *Surface Science*, 2007, **601**, 4648-4656.

39. J. J. Yeh and I. Lindau, *Atomic Data and Nuclear Data Tables*, 1985, **32**, 1-155.

105 40. J. Tang, L. Brzozowski, D. A. R. Barkhouse, X. H. Wang, R. Debnath, R. Wolowiec, E. Palmiano, L. Levina, A. G. Pattantyus-Abraham, D. Jamakosmanovic and E. H. Sargent, *ACS Nano*, 2010, **4**, 869-878.

41. NIST XPS database, http://srdata.nist.gov/xps/, Accessed 29th 110 September 2010.

42. G. Gonella, O. Cavalleri, S. Terreni, D. Cvetko, L. Floreano, A. Morgante, M. Canepa and R. Rolandi, *Surface Science*, 2004, **566-568**, 638-643.

43. J. C. Vickerman, ed., *Surface Analysis - The Principle Techniques*, 115 John Wiley & Sons, Chichester, 1997.

44. As the binding energies of the Pb 4f and S 2p levels are similar, the sampling depth (which differ by only around 0.1 nm) is taken as the same for both levels. This assumption breaks down somewhat for the most surface sensitive measurements (at 250 eV and 350 eV photon energy), where the surface composition is changing rapidly as a function of depth, and a higher proportion of oxide is probed by the more surface sensitive experiment using the S 2p signal. As the sampling depth increases, the agreement between the compositions obtained from the Pb 4f and S 2p signals improves.

45. B. R. Strohmeier, *Surface and Interface Analysis*, 1990, **15**, 51-56.